

Identified baryon and meson distributions at large transverse momenta from Au+Au collisions at $\sqrt{s_{NN}} = 200$ GeV

B.I. Abelev,⁵⁰ M.M. Aggarwal,³⁰ Z. Ahammed,⁴⁵ B.D. Anderson,²⁰ M. Anderson,⁶ D. Arkhipkin,¹³ G.S. Averichev,¹² Y. Bai,²⁸ J. Balewski,¹⁷ O. Barannikova,⁹ L.S. Barnby,² J. Baudot,¹⁸ S. Bekele,²⁹ V.V. Belaga,¹² A. Bellingeri-Laurikainen,⁴⁰ R. Bellwied,⁴⁸ F. Benedosso,²⁸ S. Bhardwaj,³⁵ A. Bhasin,¹⁹ A.K. Bhati,³⁰ H. Bichsel,⁴⁷ J. Bielcik,⁵⁰ J. Bielcikova,⁵⁰ L.C. Bland,³ S-L. Blyth,²² B.E. Bonner,³⁶ M. Botje,²⁸ J. Bouchet,⁴⁰ A.V. Brandin,²⁶ A. Bravar,³ T.P. Burton,² M. Bystersky,¹¹ R.V. Cadman,¹ X.Z. Cai,³⁹ H. Caines,⁵⁰ M. Calderón de la Barca Sánchez,⁶ J. Castillo,²⁸ O. Catu,⁵⁰ D. Cebra,⁶ Z. Chajecki,²⁹ P. Chaloupka,¹¹ S. Chattopadhyay,⁴⁵ H.F. Chen,³⁸ J.H. Chen,³⁹ J. Cheng,⁴³ M. Cherney,¹⁰ A. Chikanian,⁵⁰ W. Christie,³ J.P. Coffin,¹⁸ T.M. Cormier,⁴⁸ M.R. Cosentino,³⁷ J.G. Cramer,⁴⁷ H.J. Crawford,⁵ D. Das,⁴⁵ S. Das,⁴⁵ S. Dash,¹⁵ M. Daugherty,⁴² M.M. de Moura,³⁷ T.G. Dedovich,¹² M. DePhillips,³ A.A. Derevschikov,³² L. Didenko,³ T. Dietel,¹⁴ P. Djawotho,¹⁷ S.M. Dogra,¹⁹ W.J. Dong,⁷ X. Dong,³⁸ J.E. Draper,⁶ F. Du,⁵⁰ V.B. Dunin,¹² J.C. Dunlop,³ M.R. Dutta Mazumdar,⁴⁵ V. Eckardt,²⁴ W.R. Edwards,²² L.G. Efimov,¹² V. Emelianov,²⁶ J. Engelage,⁵ G. Eppley,³⁶ B. Erazmus,⁴⁰ M. Estienne,¹⁸ P. Fachini,³ R. Fatemi,²³ J. Fedorisin,¹² P. Filip,¹³ E. Finch,⁵⁰ V. Fine,³ Y. Fisyak,³ J. Fu,⁴⁹ C.A. Gagliardi,⁴¹ L. Gaillard,² M.S. Ganti,⁴⁵ V. Ghazikhanian,⁷ P. Ghosh,⁴⁵ J.E. Gonzalez,⁷ Y.G. Gorbunov,¹⁰ H. Gos,⁴⁶ O. Grebenyuk,²⁸ D. Grosnick,⁴⁴ S.M. Guertin,⁷ K.S.F.F. Guimaraes,³⁷ N. Gupta,¹⁹ T.D. Gutierrez,⁶ B. Haag,⁶ T.J. Hallman,³ A. Hamed,⁴⁸ J.W. Harris,⁵⁰ W. He,¹⁷ M. Heinz,⁵⁰ T.W. Henry,⁴¹ S. Hepplemann,³¹ B. Hippolyte,¹⁸ A. Hirsch,³³ E. Hjort,²² A.M. Hoffman,²³ G.W. Hoffmann,⁴² M.J. Horner,²² H.Z. Huang,⁷ S.L. Huang,³⁸ E.W. Hughes,⁴ T.J. Humanic,²⁹ G. Igo,⁷ P. Jacobs,²² W.W. Jacobs,¹⁷ P. Jakl,¹¹ F. Jia,²¹ H. Jiang,⁷ P.G. Jones,² E.G. Judd,⁵ S. Kabana,⁴⁰ K. Kang,⁴³ J. Kapitan,¹¹ M. Kaplan,⁸ D. Keane,²⁰ A. Kechechyan,¹² V.Yu. Khodyrev,³² B.C. Kim,³⁴ J. Kiryluk,²³ A. Kisiel,⁴⁶ E.M. Kislov,¹² S.R. Klein,²² A. Kocoloski,²³ D.D. Koetke,⁴⁴ T. Kollegger,¹⁴ M. Kopytine,²⁰ L. Kotchenda,²⁶ V. Kouchpil,¹¹ K.L. Kowalik,²² M. Kramer,²⁷ P. Kravtsov,²⁶ V.I. Kravtsov,³² K. Krueger,¹ C. Kuhn,¹⁸ A.I. Kulikov,¹² A. Kumar,³⁰ A.A. Kuznetsov,¹² M.A.C. Lamont,⁵⁰ J.M. Landgraf,³ S. Lange,¹⁴ S. LaPointe,⁴⁸ F. Laue,³ J. Lauret,³ A. Lebedev,³ R. Lednicky,¹³ C-H. Lee,³⁴ S. Lehocka,¹² M.J. LeVine,³ C. Li,³⁸ Q. Li,⁴⁸ Y. Li,⁴³ G. Lin,⁵⁰ X. Lin,⁴⁹ S.J. Lindenbaum,²⁷ M.A. Lisa,²⁹ F. Liu,⁴⁹ H. Liu,³⁸ J. Liu,³⁶ L. Liu,⁴⁹ Z. Liu,⁴⁹ T. Ljubicic,³ W.J. Llope,³⁶ H. Long,⁷ R.S. Longacre,³ W.A. Love,³ Y. Lu,⁴⁹ T. Ludlam,³ D. Lynn,³ G.L. Ma,³⁹ J.G. Ma,⁷ Y.G. Ma,³⁹ D. Magestro,²⁹ D.P. Mahapatra,¹⁵ R. Majka,⁵⁰ L.K. Mangotra,¹⁹ R. Manweiler,⁴⁴ S. Margetis,²⁰ C. Markert,⁴² L. Martin,⁴⁰ H.S. Matis,²² Yu.A. Matulenko,³² C.J. McClain,¹ T.S. McShane,¹⁰ Yu. Melnick,³² A. Meschanin,³² J. Millane,²³ M.L. Miller,²³ N.G. Minaev,³² S. Mioduszewski,⁴¹ C. Mironov,²⁰ A. Mischke,²⁸ D.K. Mishra,¹⁵ J. Mitchell,³⁶ B. Mohanty,⁴⁵ L. Molnar,³³ C.F. Moore,⁴² D.A. Morozov,³² M.G. Munhoz,³⁷ B.K. Nandi,¹⁶ C. Nattrass,⁵⁰ T.K. Nayak,⁴⁵ J.M. Nelson,² N.S. Nepali,²⁰ P.K. Netrakanti,⁴⁵ L.V. Nogach,³² S.B. Nurushev,³² G. Odyniec,²² A. Ogawa,³ V. Okorokov,²⁶ M. Oldenburg,²² D. Olson,²² M. Pahr,¹¹ S.K. Pal,⁴⁵ Y. Panebratsev,¹² S.Y. Panitkin,³ A.I. Pavlinov,⁴⁸ T. Pawlak,⁴⁶ T. Peitzmann,²⁸ V. Perevoztchikov,³ C. Perkins,⁵ W. Peryt,⁴⁶ S.C. Phatak,¹⁵ R. Picha,⁶ M. Planinic,⁵¹ J. Pluta,⁴⁶ N. Poljak,⁵¹ N. Porile,³³ J. Porter,⁴⁷ A.M. Poskanzer,²² M. Potekhin,³ E. Potrebenikova,¹² B.V.K.S. Potukuchi,¹⁹ D. Prindle,⁴⁷ C. Pruneau,⁴⁸ J. Putschke,²² G. Rakness,³¹ R. Raniwala,³⁵ S. Raniwala,³⁵ R.L. Ray,⁴² S.V. Razin,¹² J. Reinnarth,⁴⁰ D. Relyea,⁴ A. Ridiger,²⁶ H.G. Ritter,²² J.B. Roberts,³⁶ O.V. Rogachevskiy,¹² J.L. Romero,⁶ A. Rose,²² C. Roy,⁴⁰ L. Ruan,²² M.J. Russcher,²⁸ R. Sahoo,¹⁵ T. Sakuma,²³ S. Salur,⁵⁰ J. Sandweiss,⁵⁰ M. Sarsour,⁴¹ P.S. Sazhin,¹² J. Schambach,⁴² R.P. Scharenberg,³³ N. Schmitz,²⁴ J. Seger,¹⁰ I. Selyuzhenkov,⁴⁸ P. Seyboth,²⁴ A. Shabetai,²⁰ E. Shabaliev,¹² M. Shao,³⁸ M. Sharma,³⁰ W.Q. Shen,³⁹ S.S. Shimanskiy,¹² E.P. Sichtermann,²² F. Simon,²³ R.N. Singaraju,⁴⁵ N. Smirnov,⁵⁰ R. Snellings,²⁸ G. Sood,⁴⁴ P. Sorensen,³ J. Sowinski,¹⁷ J. Speltz,¹⁸ H.M. Spinka,¹ B. Srivastava,³³ A. Stadnik,¹² T.D.S. Stanislaus,⁴⁴ R. Stock,¹⁴ A. Stolpovsky,⁴⁸ M. Strikhanov,²⁶ B. Stringfellow,³³ A.A.P. Suaide,³⁷ N.L. Subba,²⁰ E. Sugarbaker,²⁹ M. Sumbera,¹¹ Z. Sun,²¹ B. Surrow,²³ M. Swanger,¹⁰ T.J.M. Symons,²² A. Szanto de Toledo,³⁷ A. Tai,⁷ J. Takahashi,³⁷ A.H. Tang,³ T. Tarnowsky,³³ D. Thein,⁷ J.H. Thomas,²² A.R. Timmins,² S. Timoshenko,²⁶ M. Tokarev,¹² T.A. Trainor,⁴⁷ S. Trentalange,⁷ R.E. Tribble,⁴¹ O.D. Tsai,⁷ J. Ulery,³³ T. Ullrich,³ D.G. Underwood,¹ G. Van Buren,³ N. van der Kolk,²⁸ M. van Leeuwen,²² A.M. Vander Molen,²⁵ R. Varma,¹⁶ I.M. Vasilevski,¹³ A.N. Vasiliev,³² R. Vernet,¹⁸ S.E. Vigdor,¹⁷ Y.P. Viyogi,¹⁵ S. Vokal,¹² S.A. Voloshin,⁴⁸ W.T. Waggoner,¹⁰ F. Wang,³³ G. Wang,⁷ J.S. Wang,²¹ X.L. Wang,³⁸ Y. Wang,⁴³ J.W. Watson,²⁰ J.C. Webb,⁴⁴ G.D. Westfall,²⁵ A. Wetzler,²² C. Whitten Jr.,⁷ H. Wieman,²² S.W. Wissink,¹⁷ R. Witt,⁵⁰ J. Wood,⁷ J. Wu,³⁸ N. Xu,²² Q.H. Xu,²² Z. Xu,³ P. Yepes,³⁶ I-K. Yoo,³⁴ V.I. Yurevich,¹² W. Zhan,²¹ H. Zhang,³ W.M. Zhang,²⁰ Y. Zhang,³⁸

Z.P. Zhang,³⁸ Y. Zhao,³⁸ C. Zhong,³⁹ R. Zoukarnееv,¹³ Y. Zoukarnееva,¹³ A.N. Zubarev,¹² and J.X. Zuo³⁹

(STAR Collaboration)

- ¹Argonne National Laboratory, Argonne, Illinois 60439
- ²University of Birmingham, Birmingham, United Kingdom
- ³Brookhaven National Laboratory, Upton, New York 11973
- ⁴California Institute of Technology, Pasadena, California 91125
- ⁵University of California, Berkeley, California 94720
- ⁶University of California, Davis, California 95616
- ⁷University of California, Los Angeles, California 90095
- ⁸Carnegie Mellon University, Pittsburgh, Pennsylvania 15213
- ⁹University of Illinois, Chicago
- ¹⁰Creighton University, Omaha, Nebraska 68178
- ¹¹Nuclear Physics Institute AS CR, 250 68 Řež/Prague, Czech Republic
- ¹²Laboratory for High Energy (JINR), Dubna, Russia
- ¹³Particle Physics Laboratory (JINR), Dubna, Russia
- ¹⁴University of Frankfurt, Frankfurt, Germany
- ¹⁵Institute of Physics, Bhubaneswar 751005, India
- ¹⁶Indian Institute of Technology, Mumbai, India
- ¹⁷Indiana University, Bloomington, Indiana 47408
- ¹⁸Institut de Recherches Subatomiques, Strasbourg, France
- ¹⁹University of Jammu, Jammu 180001, India
- ²⁰Kent State University, Kent, Ohio 44242
- ²¹Institute of Modern Physics, Lanzhou, China
- ²²Lawrence Berkeley National Laboratory, Berkeley, California 94720
- ²³Massachusetts Institute of Technology, Cambridge, MA 02139-4307
- ²⁴Max-Planck-Institut für Physik, Munich, Germany
- ²⁵Michigan State University, East Lansing, Michigan 48824
- ²⁶Moscow Engineering Physics Institute, Moscow Russia
- ²⁷City College of New York, New York City, New York 10031
- ²⁸NIKHEF and Utrecht University, Amsterdam, The Netherlands
- ²⁹Ohio State University, Columbus, Ohio 43210
- ³⁰Panjab University, Chandigarh 160014, India
- ³¹Pennsylvania State University, University Park, Pennsylvania 16802
- ³²Institute of High Energy Physics, Protvino, Russia
- ³³Purdue University, West Lafayette, Indiana 47907
- ³⁴Pusan National University, Pusan, Republic of Korea
- ³⁵University of Rajasthan, Jaipur 302004, India
- ³⁶Rice University, Houston, Texas 77251
- ³⁷Universidade de Sao Paulo, Sao Paulo, Brazil
- ³⁸University of Science & Technology of China, Hefei 230026, China
- ³⁹Shanghai Institute of Applied Physics, Shanghai 201800, China
- ⁴⁰SUBATECH, Nantes, France
- ⁴¹Texas A&M University, College Station, Texas 77843
- ⁴²University of Texas, Austin, Texas 78712
- ⁴³Tsinghua University, Beijing 100084, China
- ⁴⁴Valparaiso University, Valparaiso, Indiana 46383
- ⁴⁵Variable Energy Cyclotron Centre, Kolkata 700064, India
- ⁴⁶Warsaw University of Technology, Warsaw, Poland
- ⁴⁷University of Washington, Seattle, Washington 98195
- ⁴⁸Wayne State University, Detroit, Michigan 48201
- ⁴⁹Institute of Particle Physics, CCNU (HZNU), Wuhan 430079, China
- ⁵⁰Yale University, New Haven, Connecticut 06520
- ⁵¹University of Zagreb, Zagreb, HR-10002, Croatia

(Dated: August 3, 2019)

Transverse momentum spectra of π^\pm , p and \bar{p} up to 12 GeV/c at mid-rapidity in centrality selected Au+Au collisions at $\sqrt{s_{NN}} = 200$ GeV are presented. In central Au+Au collisions, both π^\pm and $p(\bar{p})$ show significant suppression with respect to binary scaling at $p_T \gtrsim 4$ GeV/c. Protons and anti-protons are less suppressed than π^\pm , in the range $1.5 \lesssim p_T \lesssim 6$ GeV/c. The π^-/π^+ and \bar{p}/p ratios show at most a weak p_T dependence and no significant centrality dependence. The p/π ratios in central Au+Au collisions approach the values in p+p and d+Au collisions at $p_T \gtrsim 5$ GeV/c. The results at high p_T indicate that the partonic sources of π^\pm , p and \bar{p} have similar energy loss when traversing the nuclear medium.

Ultra-relativistic heavy ion collisions provide a unique environment to study properties of strongly interacting matter at high temperature and energy density. When hard partons traverse the hot and dense medium created in the collision, they lose energy by gluon radiation and/or colliding elastically with surrounding partons [1, 2, 3]. This leads to a softening of the hadron spectra at high p_T . The amount of energy loss can be calculated in Quantum Chromodynamics (QCD) and is expected to be different for energetic gluons, light quarks and heavy quarks [4, 5]. Bulk particle production at low p_T is dominated by soft QCD processes and the transverse momentum (p_T) distributions are described by hydrodynamical models incorporating local thermal equilibrium and collective flow [6, 7, 8]. Between these two extreme p_T scales, distinct patterns of meson and baryon suppression have been observed [9, 10], which are consistent with hadronization through coalescence of constituent quarks from a collective partonic system [11, 12, 13, 14].

In this paper we present the p_T distributions of pions (π^\pm), protons (p) and anti-protons (\bar{p}), their nuclear modification factors, and particle ratios in 200 GeV Au+Au collisions at $0.3 < p_T < 12$ GeV/c. This explores the full range of particle production mechanisms, with emphasis on the intermediate p_T ($2 \lesssim p_T \lesssim 6$ GeV/c) range, where coalescence may play a role in hadronization, and high p_T ($p_T \gtrsim 6$ GeV/c), where particle production is dominated by jet fragmentation. Identified particles at high p_T provide direct sensitivity to differences between quark and gluon fragmentation. For example, proton and pion production at high p_T is expected to have significant contributions from quark fragmentation while anti-protons are mostly from gluon fragmentation [4, 15]. Therefore, \bar{p}/p and \bar{p}/π ratios in different systems are sensitive to the possible color charge dependence of energy loss [4]. We discuss the possible transition between jet fragmentation and quark coalescence at hadronization, the color charge dependence of the energy loss, and the fragmentation functions at high p_T .

The data used for this analysis were taken in the year 2004 by the STAR experiment [16]. A total of 15 million central triggered events for the most central bin (0-12% total cross section) and 14 million minimum-bias (MB) triggered events for the other centrality classes are used [18]. Measurements of the ionization energy loss (dE/dx) of charged tracks in the Time Projection Chamber (TPC) gas are used to identify pions (protons) in the region $p_T \leq 0.75$ (≤ 1.1) GeV/c and $2.5 \leq p_T \leq 12$ GeV/c [19, 20]. A prototype Time-of-Flight detector (TOFr) covering $\pi/30$ rad in azimuth and $-1 < \eta < 0$ in pseudorapidity [20], is also used. By combining the particle identification capability of dE/dx from the TPC and velocity from the TOFr, pions and protons can be identified up to 5 GeV/c [20, 21]. A detailed description

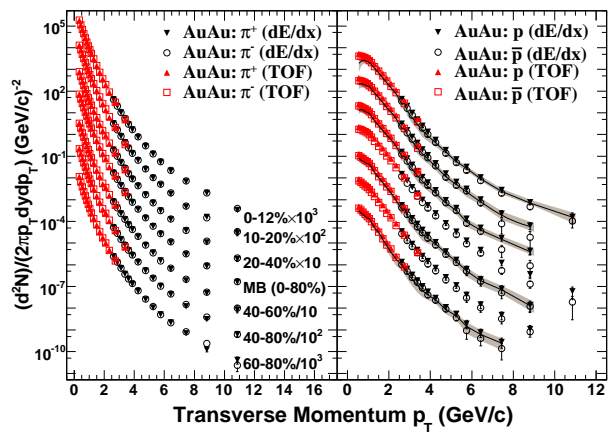


FIG. 1: Centrality dependence of mid-rapidity ($|y| < 0.5$) π^\pm , p and \bar{p} invariant yields versus p_T from 200 GeV Au+Au collisions. The error bars are the quadrature sum of statistical and systematic errors. The solid lines depict our best estimates of the proton yields corrected for the hyperon (Λ and Σ^+) feed-down [25]. The shaded bands on the lines represent the uncertainties. The order of the spectra in different centralities is the same for both panels.

of particle identification throughout the whole p_T range ($0.3 \leq p_T \leq 12$ GeV/c) can be found in [20].

At $p_T \geq 2.5$ GeV/c, the dE/dx resolution of the TPC is better than 8% and pions are separated from kaons and protons on the level of 1.5-3.0 standard deviations in dE/dx [19, 20]. The prominent yield of the pions can be extracted from a three-Gaussian fit to the inclusive positively or negatively charged hadron dE/dx distributions at given momenta [20, 22]. For protons, we used two methods. One method based on track-by-track selection, using a cut in dE/dx . The other method involved a fit of the dE/dx distribution with three Gaussians [20, 22]. For both methods, the K_S^0 measurement [9] is used to constrain the kaon contribution. The yields presented here are the results averaged from these two methods.

Acceptance and tracking efficiency are studied by Monte Carlo GEANT simulations [21, 23]. Weak-decay feed-down (e.g. $K_S^0 \rightarrow \pi^+\pi^-$) to the pion spectra was calculated using the measured K_S^0 and Λ spectra [9] and GEANT simulation. The feed-down contribution was subtracted from the pion spectra and found to be $\sim 12\%$ at $p_T = 0.35$ GeV/c, decreasing to $\sim 5\%$ for $p_T \gtrsim 1$ GeV/c. Inclusive p and \bar{p} production is presented without hyperon feed-down correction in all the figures and discussions. Protons and anti-protons from hyperon decays have similar detection efficiency as primordial p and \bar{p} at low p_T . At $p_T > 2.5$ GeV/c, the efficiency difference due to decay topology is estimated to result in $< 10\%$ correction in final inclusive yields and is corrected for. The full magnitude of the correction is assigned as a systematic uncertainty.

The invariant yields $d^2N/(2\pi p_T dp_T dy)$ of π^\pm , p and \bar{p}

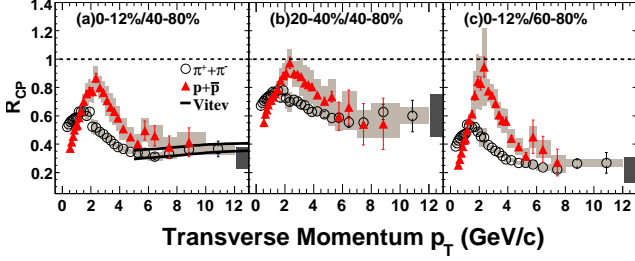


FIG. 2: Nuclear modification factors R_{CP} for $\pi^+ + \pi^-$ and $p + \bar{p}$ in 200 GeV Au+Au collisions. The point-to-point systematic uncertainties are shown as the shaded boxes around the data points. The dark shaded bands shows the normalization systematic uncertainty in the number of binary collisions. The solid lines show jet quenching predictions for pions [27].

from Au+Au collisions are shown in Fig. 1. The lines in the figure show the proton spectra after feed-down correction, to illustrate the size of the estimated feed-down contribution [23, 24, 25]. Systematic errors for the TOFr measurements are around 8% and a detailed list of contributions can be found in previous publications [21, 26]. Systematic errors for the TPC measurements are p_T dependent and include uncertainties in efficiency ($\sim 7\%$), dE/dx position and width (10-20%), K_S^0 constraint (5%), background from decay feed-down and ghost tracks (8-14%), momentum distortion due to charge build-up in the TPC volume (0-10%), the distortion of the measured spectra due to momentum resolution (0-5%) and half of the difference between the two methods to extract the proton yields (3-6%). The systematic errors are added in quadrature. The spectra from the TOFr and TPC measurements agree within systematic errors in the overlapping p_T region. The correlations of the systematic errors on the particle ratios in Fig. 2, 3 and 4 are properly taken into account.

Nuclear effects on hadron production in Au+Au collisions are quantified through comparison of the spectrum in central Au+Au collisions to 40-80% or 60-80% peripheral Au+Au collisions, scaled by the number of underlying binary nucleon-nucleon inelastic collisions (N_{bin}) calculated from a Glauber model [2], using the ratio

$$R_{CP} = \frac{d^2 N / (2\pi p_T dp_T dy) (central) / N_{bin}(central)}{d^2 N / (2\pi p_T dp_T dy) (peripheral) / N_{bin}(peripheral)}.$$

Fig. 2 shows pion ($\pi^+ + \pi^-$) and proton ($p + \bar{p}$) R_{CP} for Au+Au collisions. In 0-12% central Au+Au collisions, the pion yield shows strong suppression with R_{CP} between 0.2 and 0.4 at $p_T \gtrsim 3$ GeV/c. This is consistent with the jet quenching calculation shown in Fig. 2 (a) [27]. For each centrality, the R_{CP} values for protons peak at $p_T \sim 2-3$ GeV/c. At intermediate p_T , p and \bar{p} are less suppressed, with respect to binary scaling, than π^\pm , but a significant suppression is still observed in central Au+Au collisions. This is in contrast to nuclear modification factors in d+Au collisions, where a significant

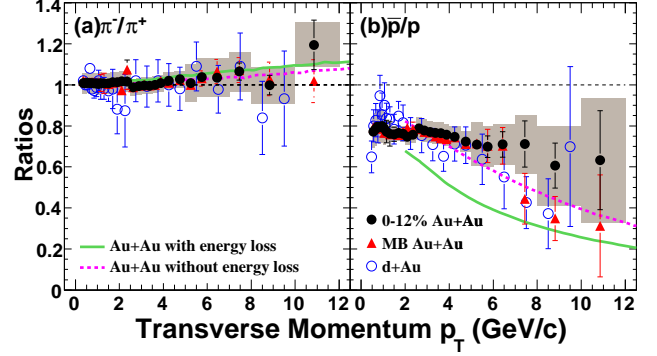


FIG. 3: The π^-/π^+ and \bar{p}/p ratios in 12% central, MB Au+Au and d+Au [21, 22] collisions at $\sqrt{s_{NN}} = 200$ GeV. The shaded boxes represent the systematic uncertainties in top 12% central Au+Au collisions. The systematic uncertainties for MB Au+Au collisions are similar. Curves are the corresponding predictions from a jet quenching model [4].

enhancement is seen for protons [22]. Previous measurements at lower transverse momentum [10] showed that R_{CP} for protons is close to 1 for $1.5 < p_T < 4.5$ GeV/c. Our results agree with those measurements within systematic errors, but our data do not suggest that R_{CP} is constant over the range $1.5 < p_T < 4.5$ GeV/c and the extended p_T reach shows that R_{CP} for protons decreases again at higher p_T .

The results in Fig. 2 clearly show different R_{CP} for protons and pions at intermediate p_T . A similar effect has been observed for K_S^0 and Λ [9], with K_S^0 (Λ) R_{CP} similar to pion (proton) R_{CP} . The grouping of particle production according to the number of constituent quarks has been attributed to quark coalescence at hadronization from a collective partonic medium [11, 12, 13, 14]. Our high statistics measurements show that these effects disappear at high p_T , where baryons and mesons show a common degree of suppression. This is consistent with the general expectation that collective and coalescence effects have a finite p_T reach.

Fig. 3 shows the π^-/π^+ and \bar{p}/p ratios in 0-12%, MB Au+Au, and d+Au [21, 22] collisions. We observe that the π^-/π^+ ratios are consistent with unity in d+Au, MB and central Au+Au collisions. Predictions from a pQCD based model with and without partonic energy loss are consistent with our data [4]. The same calculation shows a significant effect from energy loss on the \bar{p}/p ratio (Fig. 3 (b)), due to the large energy loss of gluons in the medium. Our measurements, in contrast, show little centrality dependence of the \bar{p}/p ratio at $p_T \lesssim 6$ GeV/c and a possible increase of the \bar{p}/p ratio at higher p_T in central Au+Au collisions compared to d+Au collisions.

Fig. 4 shows the p/π^+ and \bar{p}/π^- ratios in 0-12%, 60-80% Au+Au and d+Au [21, 22] collisions. The ratios in Au+Au collisions are observed to be strongly centrality dependent at intermediate p_T . In central Au+Au collisions, the p/π^+ and \bar{p}/π^- ratios peak at $p_T \sim 2-$

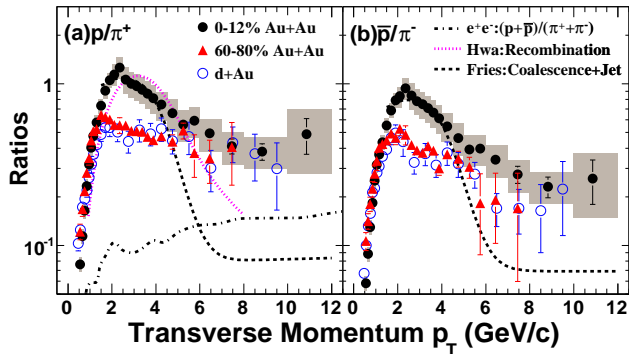


FIG. 4: The p/π^+ and \bar{p}/π^- ratios from d+Au [21, 22] and Au+Au collisions at $\sqrt{s_{NN}} = 200$ GeV. The $(p+\bar{p})/(\pi^++\pi^-)$ ratio from light quark jets in $e^+ + e^-$ collisions at $\sqrt{s} = 91.2$ GeV are shown as a dot-dashed line [29]. The shaded boxes represent the systematic uncertainties in top 12% central Au+Au collisions. The systematic uncertainties for 60-80% Au+Au collisions are similar. The dotted and dashed lines are model calculations in central Au+Au collisions [12, 13].

3 GeV/c with values close to unity, decrease with increasing p_T , and approach the ratios in d+Au, p+p and peripheral Au+Au collisions at $p_T \gtrsim 5$ GeV/c. The dotted and dashed lines are predictions for central Au+Au collisions from recombination [12] and coalescence with jet quenching and KKP fragmentation functions [13, 28] respectively. These models can qualitatively describe the $p(\bar{p})/\pi$ ratio at intermediate p_T but in general underpredict the results at high p_T .

At high p_T , the p/π^+ ratios can be directly compared to results from quark jet fragmentation as measured in $e^+ + e^-$ collisions by DELPHI [29], indicated by the dot-dashed line in Fig. 4 (a). The p/π^+ ratio measurements in d+Au and Au+Au collisions are higher than in quark jet fragmentation. This is likely due to a significant contribution from gluon jets to the proton production, which have a $(p+\bar{p})/(\pi^++\pi^-)$ ratio up to two times larger than quark jets [30]. A similar comparison cannot be made for \bar{p} production (Fig. 4 (b)), because there is a significant imbalance between quark (q) and anti-quark (\bar{q}) production at high p_T in d+Au and Au+Au collisions and the fragmentation function of q to \bar{p} can not be readily derived from $e^+ + e^-$ collisions. It is, however, known from lower beam energies, where quark fragmentation is dominant, that the \bar{p}/π and \bar{p}/p ratios from quark jets are very small (< 0.1) [22, 31]. The large \bar{p}/π^- ratio of ≈ 0.2 seen in Fig. 4 (b) is likely dominated by gluon fragmentation. This is in agreement with AKK fragmentation functions [15] which describe the STAR data in p+p collisions [22], showing that gluon fragmentation contributes to 40% of pion production at $p_T \simeq 10$ GeV/c while more than 80% of $p + \bar{p}$ are from gluon fragmentation.

At high p_T , the nuclear modification factor of protons

is similar to that of pions (Fig. 2) and the p/π^+ , \bar{p}/π^- , and \bar{p}/p ratios in central Au+Au collisions are similar to those in p+p and d+Au collisions [22]. These observations indicate that at sufficiently high p_T , fragmentation in central Au+Au and p+p events is similar and that there is no evidence of different energy loss for quarks and gluons in the medium. The theoretical calculations in Fig. 3 show that differences in radiative energy loss are expected to result in measurable changes in the \bar{p}/p and \bar{p}/π^- ratios. Those calculations, however, do not reproduce the measured p and \bar{p} spectra in p+p collisions [22], indicating that the fragmentation functions for baryon production are not well known. The determination of baryon fragmentation functions from elementary collisions and the expected range of validity of factorization for baryon production are areas of ongoing investigation [15, 22]. In addition, there is some uncertainty in the mechanism of energy loss. It has been postulated that the addition of collisional energy loss to radiative energy loss may explain the large suppression of leptons from heavy flavor decays in Au+Au collisions [32, 33]. The latest calculations [34, 35] including collisional energy loss and path length fluctuations [36] show that the nuclear modification factor of gluons is still expected to be a factor of three lower than that of light quarks.

We have reported the transverse momentum spectra of pions and protons at mid-rapidity from 200 GeV Au+Au collisions up to 12 GeV/c. Protons and anti-protons are less suppressed than pions at intermediate p_T . At $p_T \gtrsim 6$ GeV/c, both mesons and baryons are strongly suppressed. However, the relative particle abundances show no system dependence among p+p, d+Au and Au+Au collisions. These results indicate that the partonic sources of π^\pm , p and \bar{p} have similar energy loss when traversing the nuclear medium. Particle identification at high p_T provides crucial information and new challenges to the understanding of energy loss and modified parton fragmentation in strongly interacting matter.

We thank Dr. M. Djordjevic, R.J. Fries, R.C. Hwa, I. Vitev and X.N. Wang for valuable discussions and for providing the theory calculations. We thank the RHIC Operations Group and RCF at BNL, and the NERSC Center at LBNL for their support. This work was supported in part by the Offices of NP and HEP within the U.S. DOE Office of Science; the U.S. NSF; the BMBF of Germany; CNRS/IN2P3, RA, RPL, and EMN of France; EPSRC of the United Kingdom; FAPESP of Brazil; the Russian Ministry of Science and Technology; the Ministry of Education and the NNSFC of China; IRP and GA of the Czech Republic, FOM of the Netherlands, DAE, DST, and CSIR of the Government of India; Swiss NSF; the Polish State Committee for Scientific Research; SRDA of Slovakia, and the Korea Sci. & Eng. Foundation.

-
- [1] M. Gyulassy *et al.*, nucl-th/0302077; A. Kovner *et al.*, hep-ph/0304151, Review for: Quark Gluon Plasma 3, Editors: R.C. Hwa and X.N. Wang, World Scientific, Singapore.
- [2] J. Adams *et al.*, Phys. Rev. Lett. **91**, 172302 (2003).
- [3] S.S. Adler *et al.*, Phys. Rev. Lett. **91**, 072301 (2003); S.S. Adler *et al.*, Phys. Rev. Lett. **91**, 241803 (2003); B.B. Back *et al.*, Phys. Lett. B **578**, 297 (2004); I. Arsene *et al.*, Phys. Rev. Lett. **91**, 072305 (2003).
- [4] X.N. Wang, Phys. Rev. C **58**, 2321 (1998).
- [5] Y. Dokshitzer *et al.*, Phys. Lett. B **519**, 199 (2001).
- [6] D. Teaney *et al.*, nucl-th/0110037; D. Teaney *et al.*, Phys. Rev. Lett. **86**, 4783 (2001).
- [7] P. Huovinen, Nucl. Phys. A **715**, 299c (2003).
- [8] P. Kolb *et al.*, Phys. Rev. C **67**, 044903 (2003).
- [9] J. Adams *et al.*, Phys. Rev. Lett. **92**, 052302 (2004); J. Adams *et al.*, nucl-ex/0601042.
- [10] K. Adcox *et al.*, Phys. Rev. Lett. **88**, 242301 (2002); S.S. Adler *et al.*, Phys. Rev. Lett. **91**, 172301 (2003).
- [11] D. Molnar *et al.*, Phys. Rev. Lett. **91**, 092301 (2003).
- [12] R.C. Hwa *et al.*, Phys. Rev. C **70**, 024905 (2004).
- [13] R.J. Fries *et al.*, Phys. Rev. C **68**, 044902 (2003).
- [14] V. Greco *et al.*, Phys. Rev. Lett. **90**, 202302 (2003).
- [15] S. Albino *et al.*, Nucl. Phys. B **725**, 181 (2005).
- [16] K.H. Ackermann *et al.*, Nucl. Instr. Meth. A **499**, 624 (2003).
- [17] C. Adler *et al.*, Phys. Rev. Lett. **89**, 202301 (2002).
- [18] Centrality tagging follows Ref. [17]. The central trigger selected the most central 12% of the total hadronic cross section based on an on-line cut of energy deposited in the Zero-Degree Calorimeters. The pion spectra from 0-10% MB events and 0-12% central events had a 5% difference in overall scale due to the different centrality selections.
- [19] M. Anderson *et al.*, Nucl. Instr. Meth. A **499**, 659 (2003).
- [20] M. Shao *et al.*, Nucl. Instr. Meth. A **558**, 419 (2006).
- [21] J. Adams *et al.*, Phys. Lett. B **616**, 8 (2005).
- [22] J. Adams *et al.*, Phys. Lett. B **637**, 161 (2006).
- [23] C. Adler *et al.*, Phys. Rev. Lett. **87**, 262302 (2001); J. Adams *et al.*, Phys. Rev. Lett. **92**, 112301 (2004).
- [24] S. Eidelman *et al.*, Phys. Lett. B **592**, 1 (2004).
- [25] The feed-down corrections were estimated using the Λ spectra from Ref. [9] with a full simulation of decay, detection efficiency, and momentum resolution. The measured Λ spectra were extrapolated to high p_T assuming $\Lambda/p = 0.2$ at $p_T = 10$ GeV/c. The Σ^+/Λ ratio was assumed to be 0.35 [24], independent of p_T . The systematic uncertainty on the correction was calculated from the statistical and systematic uncertainties on the inclusive proton and Λ measurements, with a 30% uncertainty assigned to the extrapolated Λ spectra. An additional 20% uncertainty was assigned to account for the uncertainty in the Σ^+ yields.
- [26] L. Ruan, Ph.D. thesis, University of Science and Technology of China, 2004, nucl-ex/0503018.
- [27] I. Vitev, hep-ph/0603010, curves are calculations with initial gluon rapidity density 1150 in 0-10% Au+Au and between 100 and 150 in 40-80% Au+Au collisions.
- [28] B.A. Kniehl *et al.*, Nucl. Phys. B **597**, 337 (2001).
- [29] P. Abreu *et al.*, Eur. Phys. J. C **5**, 585 (1998).
- [30] P. Abreu *et al.*, Eur. Phys. J. C **17**, 207 (2000).
- [31] P.B. Straub *et al.*, Phys. Rev. D **45**, 3030 (1992).
- [32] S.S. Adler *et al.*, Phys. Rev. Lett. **96**, 032301 (2006).
- [33] B.I. Abelev *et al.*, nucl-ex/0607012.
- [34] M. Djordjevic *et al.*, Phys. Lett. B **632**, 81 (2006).
- [35] S. Wicks *et al.*, nucl-th/0512076.
- [36] A. Dainese *et al.*, Eur. Phys. J. C **38**, 461 (2005); K. Eskola *et al.*, Nucl. Phys. A **747**, 511 (2005).